ACS APPLIED MATERIALS & INTERFACES

Research Article

Cite This: ACS Appl. Mater. Interfaces 2019, 11, 21218−21226

www.acsami.org

Tunable, Ultrasensitive, and Flexible Pressure Sensors Based on Wrinkled Microstructures for Electronic Skins

Xiangwen Zeng,[†] Zhixuan Wang,[‡] Heng Zhang,[†] Wei Yang,[†] Li Xiang,[†] Zhizhen Zhao,[†] Lian-Mao Peng,[†] and Youfan Hu*[,†]

[†]Key Laboratory for the Physics and Chemistry of Nanodevices and Department of Electronics and [‡]Institute of Microelectronic, Peking University, Beijing 100871, China

Supporting Information

ABSTRACT: Flexible pressure sensors play an important role in electronic skins (E-Skins), which mimic the mechanical forces sensing properties of human skin. A rational design for a pressure sensor with adjustable characteristics is in high demand for different application scenarios. Here, we present tunable, ultrasensitive, and flexible pressure sensors based on compressible wrinkled microstructures. Modifying the morphology of polydimethylsiloxane (PDMS) microstructure enables the device to obtain different sensitivities and pressure ranges for different requirements. Furthermore, by intentionally introducing hollow structures in the PDMS wrinkles, our pressure sensor exhibits an ultrahigh sensitivity of 14.268 kPa^{-1}. The elastic microstructure-based capacitive sensor also possesses a very low detectable pressure limit (1.5 Pa), a fast response time (<50 ms), a wide pressure range, and excellent cycling stability. Implementing respiratory monitoring and vocalization recognition is realized by attaching the flexible pressure sensor onto the chest and throat, respectively, showing its great application potential for disease diagnosis, monitoring, and other advanced clinical/biological wearable technologies.

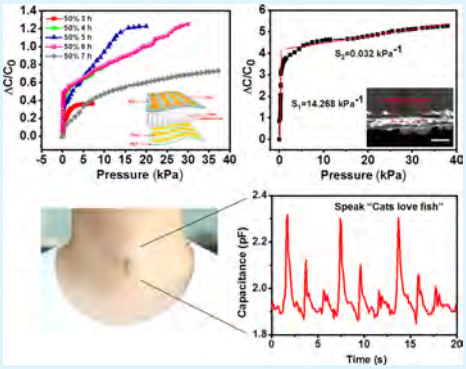

KEYWORDS: *tunable, ultrasensitive, pressure sensor, wrinkled microstructures, E-skin*

INTRODUCTION

Electronic skins (E-skins) emulate the human sophisticated somatosensory system by transducing physiological signals into electrical signals[1−4] and has great application potential in intelligence robots,[5] biomimetic prosthetics,[6] health monitoring,[7] and various wearable devices.[8] As an essential component of E-skin, pressure sensors mimic the human skin's perception of pressure. There are different types of sensory receptors with varied size, shape, number, and distribution to realize different characteristics of pressure perception in different areas of skin.[8−10] For example, the skin on the fingers and the skin on the body possess different range of receptive field and sensitivity.[11] To mimic the pressure-sensing properties of human skin, pressure sensors with different sensitivities and pressure ranges are essential for different application scenarios and functions. Realizing controllable structures to achieve a tunable sensitivity and pressure range provides a solution.

Recently, pressure sensors based on piezoresistivity,[12−15] capacitance,[16−18] or piezoelectricity,[19−21] or integrated with a field-effect transistor structure[22,23] have demonstrated high sensitivity and great flexibility. In particular, capacitive pressure sensors, which transduce mechanical strain into a capacitance change, have attracted much attention because of the advantages of the simple governing equation,[8,24] low power consumption,[8,25,26] and negligible temperature fluctuations.[27,28] Generally, elastomers are adopted as dielectric materials for their great elasticity and compressibility, which strongly affects the sensitivity and working range of a capacitive sensor. However, the viscoelastic nature of elastomers usually results in significant hysteresis and long relaxation times. To improve the performance, constructing elastomers with a porous structure has been conducted to reduce the viscoelastic behavior and to further enhance the compressibility.[29,30] Additionally, elastomers with a regularly or irregularly microstructured surface have been fabricated with an adjustable morphology for sensitivity and/or working range modifications.[9,18,31,32] However, they either require a high cost, complicated manufacturing process, or possess less controllability.

Here, we report a tunable, ultrasensitive and flexible capacitive pressure sensor based on a wrinkled polydimethylsiloxane (PDMS) microstructure via a feasible low-cost fabrication approach. The wrinkled microstructure is replicated from a reusable PDMS mold fabricated by releasing a prestretched PDMS film treated with ultraviolet ozone (UVO). The sensitivity and working range of the sensor can be tuned independently through geometry modifications of the PDMS microstructure by adjusting the PDMS mold in a well-

Received: February 12, 2019
Accepted: May 17, 2019
Published: May 17, 2019

DOI: 10.1021/acsami.9b02518
ACS Appl. Mater. Interfaces 2019, 11, 21218−21226

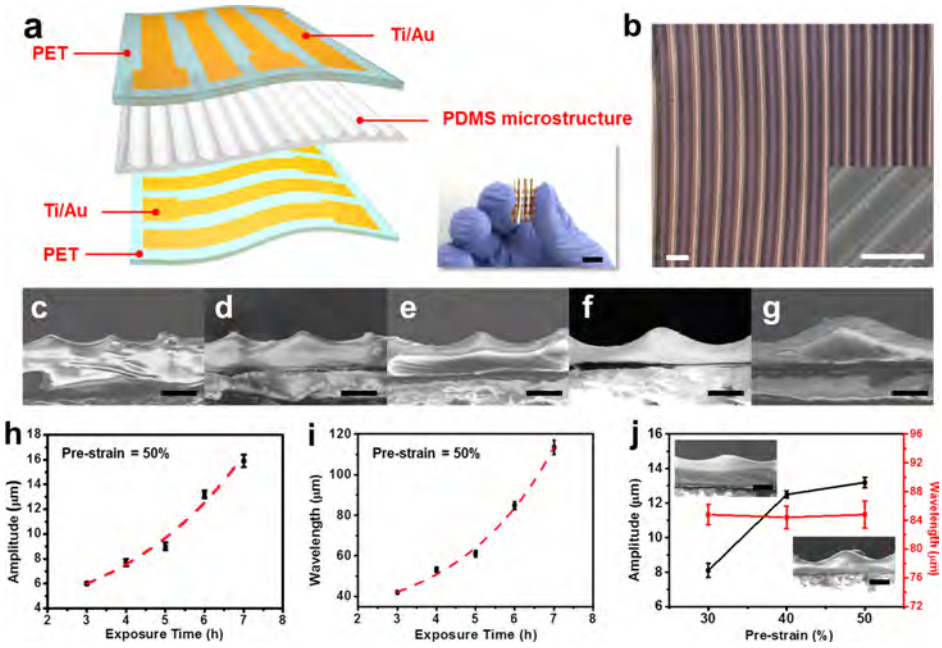

Figure 1. Wrinkled microstructure with a tunable morphology for the flexible pressure sensor. (a) Schematic structure of the pressure sensor. Inset: Photograph showing the flexibility of the device. Scale bar, 1 cm. (b) Optical image showing the uniform and regular wrinkled microstructure on the surface of PDMS. Inset: Corresponding SEM image. Scale bar, 100 μm. SEM images of microstructures replicated from PDMS molds fabricated with a pre-strain of 50% at exposure times of (c) 3 h (wavelength, 42.0 ± 0.5 μm, amplitude, 6.0 ± 0.1 μm), (d) 4 h (wavelength, 53.2 ± 1.2 μm, amplitude, 7.7 ± 0.3 μm), (e) 5 h (wavelength, 61.0 ± 1.6 μm, amplitude, 9.0 ± 0.3 μm), (f) 6 h (wavelength, 84.8 ± 1.9 μm, amplitude, 13.2 ± 0.3 μm), and (g) 7 h (wavelength, 113.5 ± 3.5 μm, amplitude, 15.9 ± 0.5 μm). Scale bar, 50 μm. (h) Amplitude−exposure time curve showing an increase in amplitude of the replicated microstructure when the PDMS mold was exposed to UVO for a longer time. (i) Wavelength−exposure time curve indicating that the wavelength of the replicated microstructure increases with an increase in the PDMS mold exposure time. (j) Wavelength−pre-strain curve (red) and amplitude−prestrain curve (black) obtained at a fixed PDMS mold exposure time of 6 h. Insets: SEM images of microstructures replicated at a pre-strain of 30% (top) and a pre-strain of 40% (bottom). Scale bar, 50 μm. Error bars in (h−j) indicate standard deviation.

controlled manner. Guided by the experimental results and the basic principle, hollow structures were introduced in the wrinkled microstructure to further reduce the elastic resistance, resulting in an ultrahigh sensitivity of 14.268 kPa^{-1}. In addition, the pressure sensor demonstrated a quite low detectable pressure limit (1.5 Pa), a fast response time (<50 ms, which was comparable with the temporal resolution of human skin[33]), and an excellent cycling stability (10 000 cycles at 0.15 kPa). The capability of monitoring the respiratory rate and recognizing different words was demonstrated by adhering the sensor onto the chest and throat, respectively, showing its promising application potential for disease diagnosis and prosthetics.

RESULTS AND DISCUSSION

Fabrication of Microstructures with a Well-Controlled Morphology. Figure 1a shows a schematic illustration of the pressure sensor, which consists of Ti/Au-patterned polyethylene terephthalate (PET) flexible substrates as top and bottom electrodes and a PDMS elastomer with a wrinkled microstructure on its surface as the dielectric layer. The bottom right of Figure 1a shows a photograph of the flexible pressure sensor. The optical image in Figure 1b and the inserted scanning electron microscopy (SEM) image present the wrinkled topography of the PDMS surface, showing a uniform and periodic microstructure, which is very beneficial for reducing viscoelastic behavior and improving the sensitivity. To obtain this wrinkled structure, a micropatterned PDMS mold was fabricated first. A PDMS film (~100 μm) was prestretched uniaxially by using a strain stage, and UVO treatment was used to turn its surface into a dense silicate layer. After releasing the applied strain, sinusoidally wrinkled microstructures were generated on the surface of PDMS because of the mismatch of elastic modulus between the relatively stiff surface layer and the more compliant elastomeric layer[34] underneath (see more details in Figure S1). Because elasticity of the PDMS's surface is greatly reduced after UVO exposure, it is necessary to transfer the microstructure generated at this step to a new PDMS film with high elasticity for constructing sensors with high performance. Figure S2 shows the cross-sectional SEM images of the original micropatterned PDMS mold and a microstructured PDMS film with the reversed pattern replicated from the mold. It shows excellent fidelity and indicates the reusability of the mold.

The UVO exposure duration can considerably affect the thickness and modulus of the surface silicate layer on the PDMS mold, and the buckling instability depends on both the pre-stretched condition and the mismatched mechanical properties between the surface and the underlying PDMS layers.[34] Thus, the geometry of the wrinkled structure on the finally obtained PDMS film can be well controlled by adjusting the pattern on the original PDMS mold by changing the pre-strain applied on the PDMS film and the duration of UVO treatment. The SEM images in Figure 1c−g show varied geometries of wrinkled microstructures with different wavelengths (λ) (42.0 ± 0.5 , 53.2 ± 1.2, 61.0 ± 1.6, 84.8 ± 1.9, and 113.5 ± 3.5 μm) and amplitudes (A) (6.0 ± 0.1, 7.7 ± 0.3,

DOI: 10.1021/acsami.9b02518
ACS Appl. Mater. Interfaces 2019, 11, 21218−21226

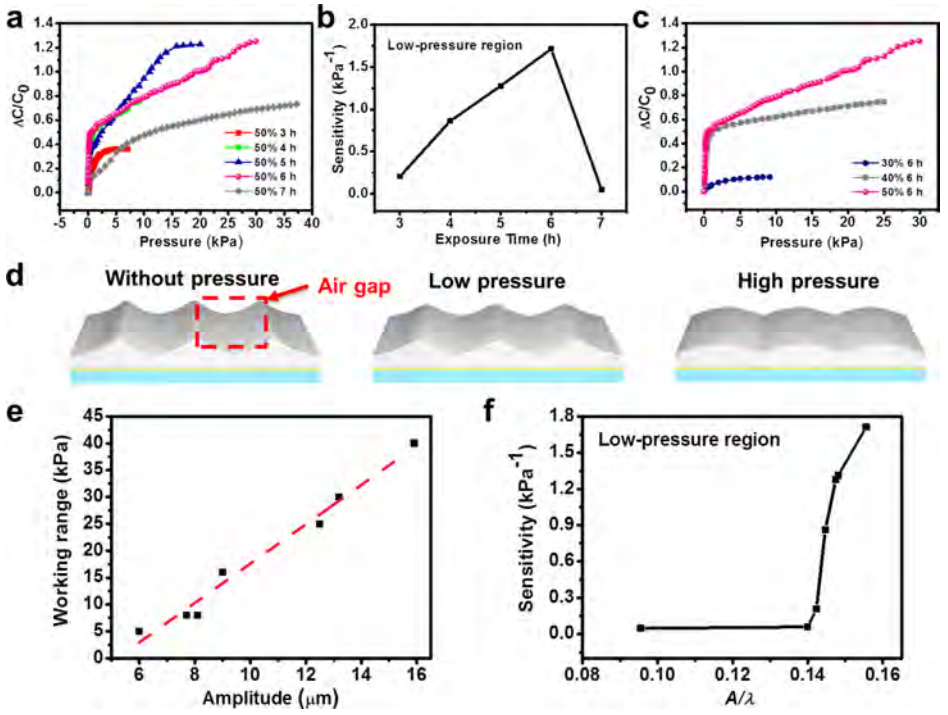

Figure 2. Pressure-sensing characterization of the sensors with varying wrinkled microstructures. (a) Relative capacitance change as a function of the pressure of the devices constructed with wrinkled microstructures replicated from PDMS mold fabricated with various exposure times at a fixed prestrain of 50%. (b) Sensitivity in the low-pressure region is plotted as a function of the exposure time of PDMS mold fabrication, showing that the sensitivity increased as the exposure time increased and peaked at 6 h. (c) Relative capacitance change as a function of pressure of the devices constructed with wrinkled microstructures replicated from the PDMS mold fabricated via different prestrains at the same exposure time of 6 h. (d) Schematic illustration of the geometry change in the wrinkled microstructure with increased pressure: without pressure, low pressure, and high pressure. (e) Working range−amplitude curve showing the increase in working range with increased amplitude of the microstructure. (f) Change in sensitivity for the low-pressure region as the aspect ratio of the microstructure, amplitude/wavelength (A/λ), increases.

9.0 ± 0.3, 13.2 ± 0.3, and 15.9 ± 0.5 μm) that were replicated from micropatterned PDMS molds prepared at the same applied pre-strain of 50% but with different UVO exposure times of 3, 4, 5, 6, and 7 h, respectively. As summarized in Figure 1h,i, when the exposure time increased, the amplitude and wavelength of the obtained microstructure significantly increased, both showing approximately exponential relationships with the exposure time.

Another adjustable parameter is the strain applied on the PDMS film during mold fabrication. We should mention that when the applied strain is below 30%, it is difficult to produce a uniformly microstructured mold, whereas when the applied strain is above 50%, cracks will form in the PDMS mold because of the high inner stress. Figure 1j shows that when the UVO exposure time was maintained at 6 h, the amplitude of the replicate microstructure increased (from 8.1 ± 0.4, 12.5 ± 0.2 to 13.2 ± 0.3 μm) as the applied pre-strain increased from 30 to 50%, while the wavelength of the microstructure was almost unchanged (84.8 ± 1.4, 84.4 ± 1.6, and 84.8 ± 1.9 μm). The upper and bottom SEM images inserted in Figure 1j show the microstructures replicated from molds obtained at pre-strains of 30 and 40%, respectively. Therefore, the wavelength and amplitude of the obtained replicate microstructure can be controlled separately by adjusting the UVO exposure time and the applied pre-strain during PDMS mold fabrication, respectively, which enables the construction of a tunable pressure sensor and highlights the advantage of the proposed approach.

Tuning the Sensitivity and Working Range of the Pressure Sensor. Compared with traditional fabrication methods, such as multistep photolithography,[23,35] the fabrication process for a pressure sensor based on a wrinkled microstructure is simple and cost-effective, as illustrated in Figure S3. In brief, PDMS was spin-coated on a PET substrate with striped electrodes; then, a prepared PDMS mold was pressed onto it. After curing and peeling off the mold, the wrinkled microstructure was replicated on the spin-coated PDMS. Finally, another PET substrate with striped electrodes was placed on the wrinkle microstructure, making the top and bottom striped electrodes orthogonal. These two electrodes could be well bonded to the PDMS due to the PDMS's good viscosity, forming a capacitive pressure sensor. The capacitance of a parallel-plate capacitive sensor is determined by $C = \varepsilon_r\varepsilon_0 A/d$, where ε_r is the relative permittivity of the dielectric layer, ε_0 is the permittivity of vacuum, A is the area where the plates overlap each other, and d is the distance between the two plates. The change in d under an applied pressure leads to a change in capacitance, which can be quantified and utilized for pressure sensing. As shown in Figure 2a, devices constructed with different microstructured PDMS were evaluated, which were replicated from PDMS molds fabricated at exposure times of 3, 4, 5, 6, and 7 h with the same pre-strain of 50%, respectively. All data presented here were cut off at certain values of applied pressure accordingly, where the change in capacitance was negligible (<0.01 pF) when the applied pressure was further increased. The pressure range before this value can be defined as the working range of the pressure sensor. Clearly, the change in capacitance of all devices undergoes a sharp slope in the low-pressure region and a gentle slope in the high-pressure region. The pressure

DOI: 10.1021/acsami.9b02518
ACS Appl. Mater. Interfaces 2019, 11, 21218−21226

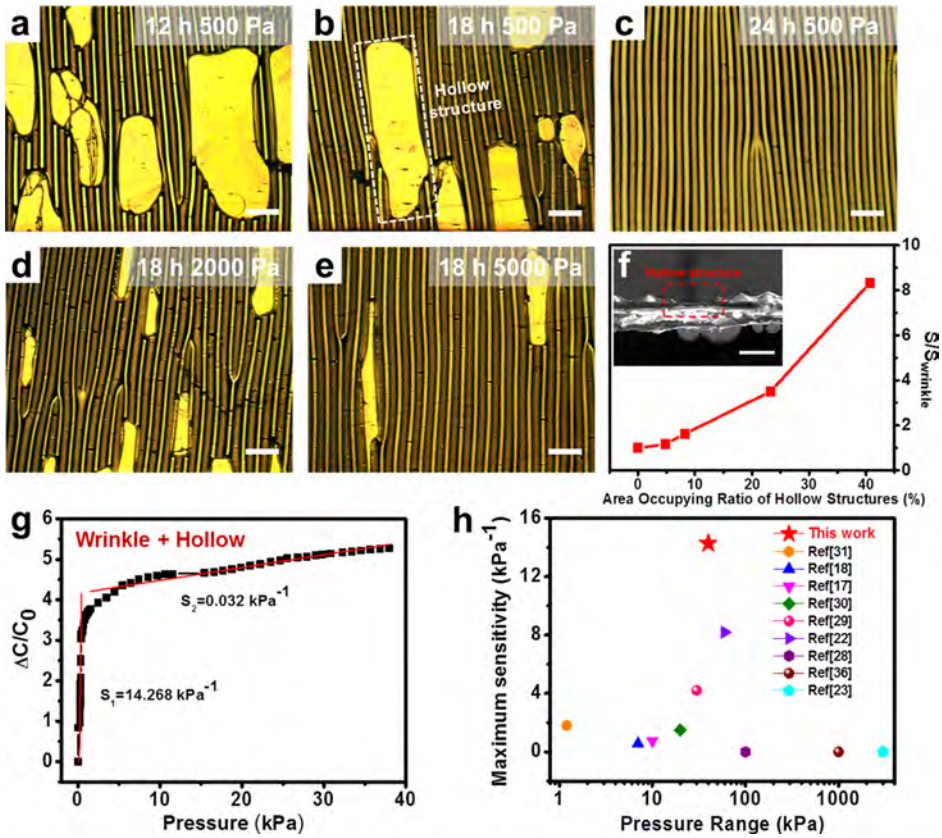

Figure 3. Hollows in the PDMS wrinkled microstructures. (a–c) Optical images of different densities of hollow structures in the wrinkled microstructure for precuring times of 12, 18, and 24 h (at the same applied pressure of 500 Pa). Scale bar, 200 μm. (d,e) Optical images of different densities of hollow structures in the wrinkled microstructure for applied pressures of 2000 and 5000 Pa (at the same precuring time of 18 h). Scale bar, 200 μm. (f) Normalized sensitivity of the device ($S/S_{wrinkle}$) increased as the area occupying ratio of the hollow structure increased. Insets: SEM image of the hollow structure in the wrinkled microstructures. Scale bar, 100 μm. (g) Relative capacitance change as a function of pressure of the constructed device showing an unprecedented high sensitivity. (h) Pressure-sensing performance comparison of this work with previous reports.

sensitivity can be defined as the slope of the traces, $S = \frac{\delta\left(\frac{\Delta C}{C_0}\right)}{\delta P}$, where ΔC and C_0 are the variation of capacitance and the initial capacitance without pressure, respectively, and P is the applied pressure. The sensitivity of these devices in the low-pressure region is plotted in Figure 2b. First, the sensitivity increased almost linearly with an increase in UVO exposure time for treating the PDMS mold. Then, it reached a maximum of 1.713 kPa^{-1} at a UVO exposure time of 6 h and subsequently decreased when the UVO exposure time was further increased.

As discussed in the previous section, both the amplitude and wavelength of the obtained microstructure increased with increased UVO exposure time during the mold fabrication. The experimental results reveal that the sensitivity of the sensor was optimized at certain microstructure morphologies. To further investigate the effect of amplitude and wavelength on the device's performance separately, we fabricated sensors with wrinkled microstructures of the same wavelength but different amplitudes by utilizing molds obtained with different applied pre-strains at the optimum exposure time of 6 h. Figure 2c shows the test results of these sensors. The highest sensitivity and the largest pressure range was obtained for the microstructure with the largest amplitude, which was replicated from the PDMS mold fabricated with a pre-strain of 50% (Figure S4).

To determine the underlying mechanism, Figure 2d schematically shows the change in geometry of the wrinkled microstructure under an increased pressure. First, the sensitivity of the sensor was greatly enhanced by introducing air gaps in the dielectrics with a microstructured PDMS film compared with an unstructured one, as shown in Figure S5, which resulted in an elevated compressibility by reducing the elastic resistance of the dielectric layer.[18] In addition, when a microstructured PDMS film is compressed, a reduction in air gap volumes will lead to an increased effective dielectric constant, which further enhances the change rate of capacitance and, thus, the pressure sensitivity. Because the air gap volume at the upper part of the microstructure is larger than that at the bottom, the top of the microstructure has a smaller effective mechanical modulus and greater compressibility. At a relatively low pressure, the distance between the top and bottom electrodes was considerably reduced by the deformation occurring primarily at the top of the microstructure, resulting in a large change rate in capacitance with pressure, that is, a higher sensitivity. At a high pressure, the compressed microstructure became more flat. Its compressibility became lower because of the reduced air gap volume in the PDMS microstructure, and there was a reduced change rate in capacitance with pressure, corresponding to a reduced sensitivity for the device. Therefore, we expect that a larger pressure range should be obtained for a device based on a

DOI: 10.1021/acsami.9b02518
ACS Appl. Mater. Interfaces 2019, 11, 21218–21226

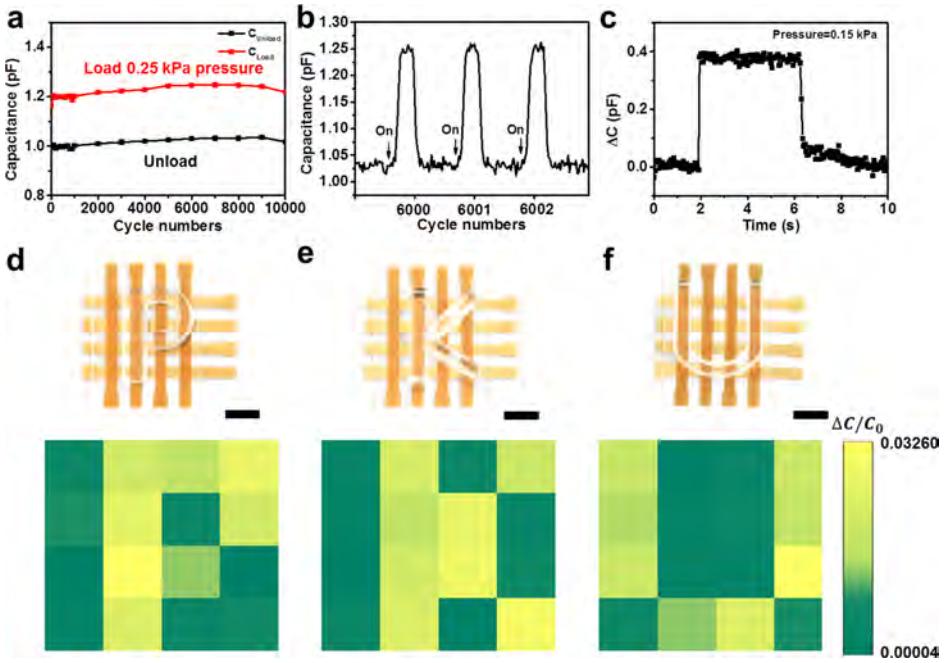

Figure 4. Stability, response time of the device, and pressure mapping. (a) Capacitance change of the pressure sensor for 10 000 loading (0.25 kPa)−unloading cycles. (b) Enlarged fragment during the 6001st to 6003rd cycle. (c) Response and relaxation test upon loading and unloading at 0.15 kPa, exhibiting a response time of 50 ms and a relaxation time < 0.2 s. Mapping of pressure distributions on the 4 × 4 sensor array upon placing (d) an acrylic board with the "P" shape (0.19 g), (e) an acrylic board with the "K" shape (0.118 g), and (f) an acrylic board with the "U" shape (0.124 g). Each panel includes an optical image (top) and the response of the sensor pixels (bottom).

microstructure with a larger amplitude, and a higher sensitivity should be realized with a microstructure that possesses a higher air gap volume, especially in the low-pressure region.

Figure 2e summarizes the working ranges and the corresponding microstructure's amplitudes for all tested devices. As expected, there is a nearly linear relationship between them. Aspect ratio (A/λ) was used to evaluate and compare the air gap volume in different microstructures, which is positively correlated with the ratio of air gap volume/microstructure volume (Figure S6 and Supporting Information Note). Figure 2f shows that in the low-pressure region, the sensitivity increased as the A/λ increased in the tested devices. As a result, the pressure range of the sensor can be adjusted by modifying the amplitude of the microstructure, whereas the sensitivity can be tuned by the value of A/λ. This shows great adaptability for different applications where different sensitivities and working ranges are required.

Hollows in the Wrinkled Microstructure. To further enhance the sensitivity, increasing the aspect ratio of the microstructure could be performed. However, the structure becomes shaper and sharper as the A/λ increases, which quickly meets its limitation because of mechanical instability or failure. From a more fundamental point of view, the air gap volume in the microstructure is the primary determiner of the effective mechanical modulus and, thus, the compressibility and sensitivity. Therefore, introducing hollow structures in the wrinkled microstructure to further increase the volume ratio of the air gap is a better solution to achieve a much higher sensitivity. Residual air in the PDMS mold during the replicate process was utilized to rationally produce hollow structures in the obtained wrinkled microstructure with an adjustable density by changing the precuring time of the PDMS or the applied pressure during replication (more details in the Methods). Optical images of the obtained structures are shown in Figure 3a−e. They reveal that the density of the hollow structure decreased as the precuring time of the PDMS increased when the applied pressure between the mold and the PDMS was constant (500 Pa in this case) or as the applied pressure increased when the precuring time of the PDMS was constant (18 h in this case). Thus, the denser the PDMS mixture or the greater the pressure is, the less amount of residual air is obtained. An SEM image of the cross-sectional view of the hollow structure is shown in the insert of Figure 3f in which the wavelength and the amplitude of the wrinkled microstructure was measured to be 85.6 ± 1.5 and 13.3 ± 0.5 μm, respectively.

Sensors constructed on these structures were evaluated. Figure 3f shows that the normalized sensitivity of the device ($S/S_{wrinkle}$), where $S_{wrinkle}$ is the sensitivity obtained from the device with only the wrinkle structures, increased quickly as the area-occupying ratio of the hollow structures increased. The pressure response from the device with the best performance is shown in Figure 3g. It shows an ultrahigh sensitivity of 14.268 kPa^{-1} in the low-pressure region (<0.7 kPa) and 0.032 kPa^{-1} in the high-pressure region (0.7−40 kPa) and a large working range (40 kPa). In particular, the sensitivity was boosted almost one order of magnitude over the one without the hollow structure. Figure 3h shows the sensitivity and pressure range of this device, compared with those of pressure sensors in previous reports.[17,18,22,23,28−31,36] Obviously, our device exhibits the highest sensitivity and a relatively large pressure range simultaneously. Moreover, our device exhibits an ultralow detectable pressure limit of 1.5 Pa, benefiting from the considerably reduced effective mechanical modulus because of the introduction of hollow structures, as shown in Figure S7. The performance and corresponding geometry of the microstructure of all devices we tested are summarized in Table S1.

DOI: 10.1021/acsami.9b02518
ACS Appl. Mater. Interfaces 2019, 11, 21218−21226

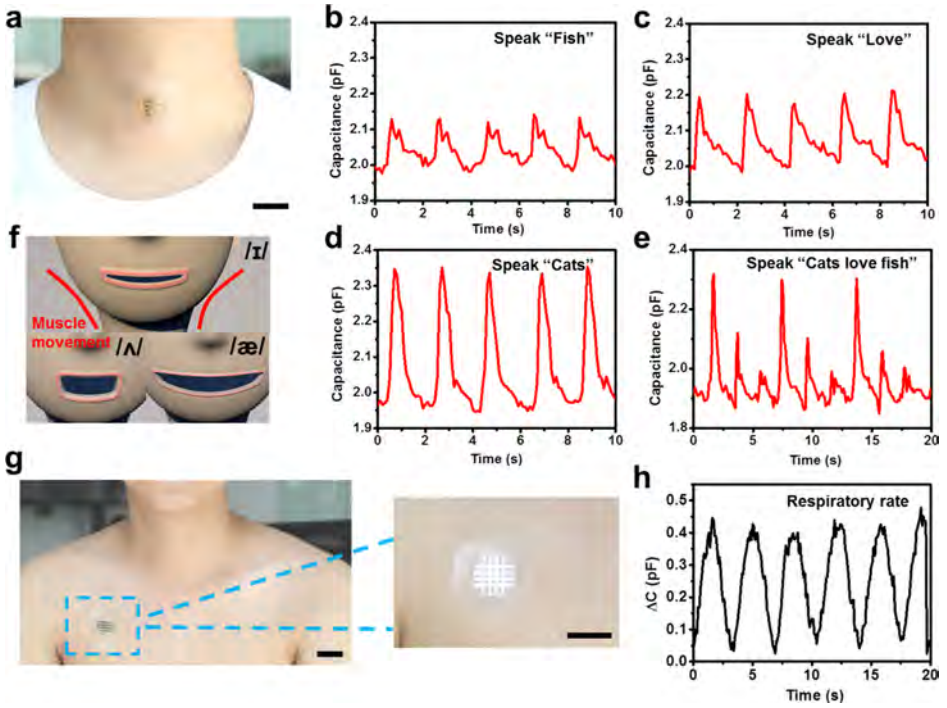

Figure 5. Vocalization recognition test and respiration rate measurement for biological application. (a) Photograph of mounting a flexible sensor onto a human throat for the vocalization recognition test. Scale bar, 2.5 cm. (b–e) Changes in capacitance when speaking "Fish", "Love", "Cats", and "Cats love fish". (f) Schematic illustration of the mouth shape corresponding to the three kinds of phonetic symbols: /ɪ/, /Λ/, and /æ/. (g) Photograph of a flexible sensor attached to a human chest for respiration rate measurement. Scale bar, 2.5 cm. (h) Capacitance change during respiration.

Stability, Response Time of the Device, and Pressure Mapping. To check the stability of our device, we performed repetitive tests to load–unload a pressure of 0.25 kPa on the device for 10 000 cycles. The capacitance change of the device was sampled every 100 cycles before the 1000th cycle and then sampled every 1000 cycles afterwards. The fluctuation of the measured capacitance under repeated loading and unloading statuses was less than 7%, as shown in Figure 4a, and with an enlarged fragment during the 6001st to 6003rd cycle, as shown in Figure 4b, which demonstrated an excellent mechanical stability that is comparable to the device without microstructures (Figure S9). Introducing microstructures into the elastomer can effectively reduce its viscoelastic behavior and thus promote the sensor's speed (Figure S10). As shown in Figure 4c, our device exhibits a fast response time of 50 ms, which is comparable with the temporal resolution of human skin (20–40 ms).[33] The relaxation time of the device (<0.2 s) is also much lower than that of the previously reported unstructured PDMS (≫1 s).[17,18] In addition, a 4 × 4 sensor array based on two orthogonal electrodes with an area of 1.6 × 2.4 cm^2 (area of each pixel is 1.5 × 1.5 mm^2) was fabricated to conduct a pressure mapping test. Figure 4d–f show the optical images and the corresponding capacitance changes of each pixel recorded upon placing "P", "K", and "U" letters on the sensor array. These letters were made of acrylic materials with weights of 0.19, 0.118, and 0.124 g. The letter figure can be clearly seen from the mapping, and the crosstalk between pixels is quite small.

Applications in Human Physiology Monitoring. Because of the advantages of high sensitivity and fast response speed, these devices can be used for real-time pressure recording applications, such as human physiology monitoring. First, we performed vocalization recognition test by mounting the flexible sensor onto a human throat, as shown in Figure 5a. Generally, the voice is produced by vibrations of the vocal cords in the larynx, which create fluctuations in air pressure from the lungs to generate sound waves. The waveforms can be modified by the resonances in the vocal tract according to the position and shape of the mouth, soft palate, and other speech organs, thus forming different sounds.[37,38] The vibration of the vocal cords and the opening and closing of the mouth causes the movement of muscles and thus the deformation of the epidermis around the jaw and throat. Because the intensity of sound depends on the amplitude of the vocal cords' vibration, we controlled the sound at approximately 90 dB during the test, which maintained similar vibration amplitude, to eliminate different epidermis deformations caused by different vocal cord vibration intensities. Figure 5b–d show that when speaking the words "Fish", "Love", and "Cats", there was a capacitance change of 0.1, 0.2, and 0.4 pF in the device, respectively, and different patterns of signals were obtained. Therefore, vocalization recognition was able to be performed when speaking "Cats love fish", as shown in Figure 5e. The distinct signal level and different signal patterns can be explained by distinct deformations experienced by the device because of different epidermis deformations when speaking different words (Figure S11). As shown in Figure 5f, during pronouncing the word "Fish", it includes a vowel /ɪ/ and is pronounced with a small mouth opening. This results in little muscle movement and small deformation in the epidermis, whereas the word "Cats" with the vowel of /æ/ has a larger mouth opening, and the mouth stretched substantially to both sides, leading to the largest muscle movement and greatest deformation in the epidermis. In addition, the final consonants of these words lead to different patterns of signals because of different muscle movements. It should be clarified that during

DOI: 10.1021/acsami.9b02518
ACS Appl. Mater. Interfaces 2019, 11, 21218–21226

the test the sound volume will affect the measured absolute capacitance change in the device caused by speaking, but the relative capacitance change between speaking different words and the different patterns obtained when speaking different words will maintain, which is the principle for speech recognition here. Thus, different words can be recognized "spoken" by the people through different epidermis deformations caused by different shapes of the mouth without having to make a sound. Therefore, via further optimization, these devices could be used for more accurate speech recognition, which can benefit people with damaged vocal cords.

Respiratory rate is an important biological signal that provides information about the physiological condition of the human body and is an indicator of various illnesses.[39] For example, tachypnea may be an early medical sign of pneumonia in children and shortness of breath is one of the symptoms of asthma. As shown in Figure 5g, we attached a pressure sensor onto the chest for respiration rate measurement. During inhalation, the chest expands forward, which results in compression of the sensor and causes an increase in the capacitance of the sensor. Then, during exhalation, the chest recovers to its original position, and the sensor regains its original capacitance. As shown in Figure 5h, the recorded data reveals a respiration rate of approximately 18 breaths per minute, which conforms to the typical respiratory rate of a healthy adult at rest.[40]

CONCLUSIONS

In summary, we have presented a tunable pressure sensor with ultrahigh sensitivity based on a wrinkled microstructure. By changing the aspect ratio and amplitude of the microstructure in a controllable manner, the sensitivity and working range can be tuned, respectively. The sensor with the sharpest microstructure shape achieved the highest sensitivity of 1.713 kPa^{-1}. By introducing hollow structures into the wrinkles to further increase the air gap volume and reduce the effective mechanical modulus, an ultrahigh sensitivity of 14.268 kPa^{-1} was demonstrated. With the help of the highly compressible microstructure, the device also exhibits quite a low detectable pressure limit (1.5 Pa), a fast response times (<50 ms), a wide pressure range, and excellent cycling stability. Vocalization recognition and respiratory rate monitoring have been demonstrated as examples of human physiology monitoring applications, which shows promising potential for applications in disease diagnosis, prosthetics, and various wearable devices.

EXPERIMENTAL SECTION

Microstructure Mold Fabrication. The base agent and curing agent of PDMS (Sylgard 184, Dow Corning) were mixed at a weight ratio of 10:1, which was well blended and deaerated via a planetary centrifugal mixer (Thinky, AR-100) for 15 min. Then, the mixture was spin-coated at 500 rpm for 60 s on a PET substrate and was cured at 80 °C for 3 h. After curing, the cured PDMS film (thickness: ~100 μm) was peeled-off from PET and stretched uniaxially on a strain stage, followed by UVO exposure. Finally, the wrinkled microstructure was generated on the PDMS surface after releasing the applied pre-strain.

Pressure Sensor Fabrication. First, 10 nm of Ti and 50 nm of Au were deposited on UVO-treated PET substrates to form flexible electrodes using a PET mask, which was fabricated by a laser cutting machine (Universal Laser Systems, PLS 6MW). The base agent and curing agent of PDMS were mixed at a weight ratio of 10:1 and were spin-coated at 3000 rpm for 60 s on the electrode-patterned PET substrates after blending and deaeration. After curing at room temperature for 24 h, the PDMS presented a semisolid state. The microstructure mold was placed on the PDMS-coated PET substrate. A pressure of 500 Pa was applied to clamp the entire stack and remove the residual air. Then, the stack was baked at 80 °C for 6 h. The microstructured PDMS with the reversed wrinkle pattern was generated after peeling off the mold. Finally, another PET substrate with Ti/Au electrodes was added on with an orientation orthogonal to the Ti/Au electrodes on the bottom PET substrate, forming 4 × 4 sensor arrays.

Fabrication of the Hollow Structure. Different densities for the hollow structure can be obtained via two approaches as follows. *Changing the precuring condition*: The PDMS film that was spin-coated on the PET substrate was precured at room temperature for different times (at least for 12 h) to obtain different curing degrees. Then, a micropatterned mold was placed on top. The entire stack was clamped at a pressure of 500 Pa and was baked at 80 °C for 10 h. *Changing the applied pressure*: The PDMS film that was spin-coated on the PET substrate was precured at room temperature for 18 h. Then, a micropatterned mold was placed on top. The entire stack was clamped at different pressures and was baked at 80 °C for 10 h. The micropatterned mold used here was fabricated with an exposure time of 6 h and a pre-strain of 50%.

Characterization of the Pressure Sensor. The capacitance of the pressure sensor was measured by using an Agilent 4294A Precision Impedance Analyzer. A universal high-performance motion controller (XPS-Q8) and force gauge (Handpi, HP-5) were used to apply the pressure.

ASSOCIATED CONTENT

Supporting Information

The Supporting Information is available free of charge on the ACS Publications website at DOI: 10.1021/acsami.9b02518.

Schematic illustration of the fabrication process of microstructured PDMS film; cross-sectional SEM image of a micropatterned PDMS mold and the replicated PDMS film from it; schematic illustration of the fabrication process of microstructured flexible pressure sensor; sensitivity at low pressure region and working range versus pre-strain applied during mold fabrication; relative capacitance change with respect of pressure for unstructured and microstructured device; change of capacitance under loading−unloading of 1.5 Pa pressure; schematic illustration of wrinkled microstructure; capacitance change of a pressure sensor without microstructures for 10 000 loading−unloading cycles; response and relaxation test of sensors based on microstructured PDMS films with different volume ratios of air gap and unstructured PDMS films upon loading and unloading at 0.15 kPa; measuring deformation of the epidermis caused by muscle movement when speaking; calculation of the volume ratio of the air gap to the microstructure layer; and performance of pressure sensors based on wrinkled microstructure and the corresponding geometry of the microstructure (PDF)

Video recording vocalization recognition test (MP4)

AUTHOR INFORMATION

Corresponding Author

*E-mail: youfanhu@pku.edu.cn.

ORCID

Youfan Hu: 0000-0001-9798-1631

Notes

The authors declare no competing financial interest.

DOI: 10.1021/acsami.9b02518
ACS Appl. Mater. Interfaces 2019, 11, 21218−21226

■ ACKNOWLEDGMENTS

This work was supported by the National Natural Science Foundation of China (grant nos. 61571016 and 61621061) and the National Key Research & Development Program (grant no. 2016YFA0201901).

■ REFERENCES

(1) Kim, D.-H.; Lu, N.; Ma, R.; Kim, Y.-S.; Kim, R.-H.; Wang, S.; Wu, J.; Won, S. M.; Tao, H.; Islam, A.; Yu, K. J.; Kim, T.-i.; Chowdhury, R.; Ying, M.; Xu, L.; Li, M.; Chung, H.-J.; Keum, H.; McCormick, M.; Liu, P.; Zhang, Y.-W.; Omenetto, F. G.; Huang, Y.; Coleman, T.; Rogers, J. A. Epidermal Electronics. *Science* **2011**, *333*, 838−843.

(2) Pan, L.; Chortos, A.; Yu, G.; Wang, Y.; Isaacson, S.; Allen, R.; Shi, Y.; Dauskardt, R.; Bao, Z. An Ultra-Sensitive Resistive Pressure Sensor Based on Hollow-Sphere Microstructure Induced Elasticity in Conducting Polymer Film. *Nat. Commun.* **2014**, *5*, 3002.

(3) Ramuz, M.; Tee, B. C.-K.; Tok, J. B.-H.; Bao, Z. Transparent, Optical, Pressure-Sensitive Artificial Skin for Large-Area Stretchable Electronics. *Adv. Mater.* **2012**, *24*, 3223−3227.

(4) Wang, C.; Hwang, D.; Yu, Z.; Takei, K.; Park, J.; Chen, T.; Ma, B.; Javey, A. User-Interactive Electronic Skin for Instantaneous Pressure Visualization. *Nat. Mater.* **2013**, *12*, 899−904.

(5) Jeong, J.-W.; Yeo, W.-H.; Akhtar, A.; Norton, J. J. S.; Kwack, Y.-J.; Li, S.; Jung, S.-Y.; Su, Y.; Lee, W.; Xia, J.; Cheng, H.; Huang, Y.; Choi, W.-S.; Bretl, T.; Rogers, J. A. Materials and Optimized Designs for Human-Machine Interfaces Via Epidermal Electronics. *Adv. Mater.* **2013**, *25*, 6839.

(6) Tee, B. C.-K.; Chortos, A.; Berndt, A.; Nguyen, A. K.; Tom, A.; McGuire, A.; Lin, Z. C.; Tien, K.; Bae, W.-G.; Wang, H.; Mei, P.; Chou, H.-H.; Cui, B.; Deisseroth, K.; Ng, T. N.; Bao, Z. A skin-inspired organic digital mechanoreceptor. *Science* **2015**, *350*, 313−316.

(7) Chen, L. Y.; Tee, B. C.-K.; Chortos, A. L.; Schwartz, G.; Tse, V.; Lipomi, D. J.; Wong, H.-S. P.; McConnell, M. V.; Bao, Z. Continuous Wireless Pressure Monitoring and Mapping with Ultra-Small Passive Sensors for Health Monitoring and Critical Care. *Nat. Commun.* **2014**, *5*, 5028.

(8) Hammock, M. L.; Chortos, A.; Tee, B. C.-K.; Tok, J. B.-H.; Bao, Z. 25th Anniversary Article: The Evolution of Electronic Skin (E-Skin): A Brief History, Design Considerations, and Recent Progress. *Adv. Mater.* **2013**, *25*, 5997−6038.

(9) Tee, B. C.-K.; Chortos, A.; Dunn, R. R.; Schwartz, G.; Eason, E.; Bao, Z. Tunable Flexible Pressure Sensors using Microstructured Elastomer Geometries for Intuitive Electronics. *Adv. Funct. Mater.* **2014**, *24*, 5427−5434.

(10) Delmas, P.; Hao, J.; Rodat-Despoix, L.; Rodat-Despoix, L. Molecular Mechanisms of Mechanotransduction in Mammalian Sensory Neurons. *Nat. Rev. Neurosci.* **2011**, *12*, 139−153.

(11) Johansson, R. S.; Flanagan, J. R. Coding and use of Tactile Signals from the Fingertips in Object Manipulation Tasks. *Nat. Rev. Neurosci.* **2009**, *10*, 345−359.

(12) Gong, S.; Schwalb, W.; Wang, Y.; Chen, Y.; Tang, Y.; Si, J.; Shirinzadeh, B.; Cheng, W. A Wearable and Highly Sensitive Pressure Sensor with Ultrathin Gold Nanowires. *Nat. Commun.* **2014**, *5*, 3132.

(13) Pang, C.; Lee, G.-Y.; Kim, T.-I.; Kim, S. M.; Kim, H. N.; Ahn, S.-H.; Suh, K.-Y. A Flexible and Highly Sensitive Strain-Gauge Sensor Using Reversible Interlocking of Nanofibers. *Nat. Mater.* **2012**, *11*, 795−801.

(14) Lee, J.; Kwon, H.; Seo, J.; Shin, S.; Koo, J. H.; Pang, C.; Son, S.; Kim, J. H.; Jang, Y. H.; Kim, D. E.; Lee, T. Conductive Fiber-Based Ultrasensitive Textile Pressure Sensor for Wearable Electronics. *Adv. Mater.* **2015**, *27*, 2433.

(15) Wang, L.; Li, Y. A Review for Conductive Polymer Piezoresistive Composites and a Development of a Compliant Pressure Transducer. *IEEE Transactions on Instrumentation and Measurement*, 2013; Vol. *62*, pp 495−502.

(16) Lei, Z.; Wang, Q.; Sun, S.; Zhu, W.; Wu, P. A Bioinspired Mineral Hydrogel as a Self-Healable, Mechanically Adaptable Ionic Skin for Highly Sensitive Pressure Sensing. *Adv. Mater.* **2017**, *29*, 1700321.

(17) Boutry, C. M.; Nguyen, A.; Lawal, Q. O.; Chortos, A.; Rondeau-Gagné, S.; Bao, Z. A Sensitive and Biodegradable Pressure Sensor Array for Cardiovascular Monitoring. *Adv. Mater.* **2015**, *27*, 6954−6961.

(18) Mannsfeld, S. C. B.; Tee, B. C.-K.; Stoltenberg, R. M.; Chen, C. V. H.-H.; Barman, S.; Muir, B. V. O.; Sokolov, A. N.; Reese, C.; Bao, Z. Highly Sensitive Flexible Pressure Sensors with Microstructured Rubber Dielectric Layers. *Nat. Mater.* **2010**, *9*, 859−864.

(19) Pan, C.; Dong, L.; Zhu, G.; Niu, S.; Yu, R.; Yang, Q.; Liu, Y.; Wang, Z. L. High-Resolution Electroluminescent Imaging of Pressure Distribution Using a Piezoelectric Nanowire LED Array. *Nat. Photonics* **2013**, *7*, 752−758.

(20) Dagdeviren, C.; Su, Y.; Joe, P.; Yona, R.; Liu, Y.; Kim, Y.-S.; Huang, Y.; Damadoran, A. R.; Xia, J.; Martin, L. W.; Huang, Y.; Rogers, J. A. Conformable Amplified Lead Zirconate Titanate Sensors with Enhanced Piezoelectric Response for Cutaneous Pressure Monitoring. *Nat. Commun.* **2014**, *5*, 4496.

(21) Persano, L.; Dagdeviren, C.; Su, Y.; Zhang, Y.; Girardo, S.; Pisignano, D.; Huang, Y.; Rogers, J. A. High Performance Piezoelectric Devices Based on Aligned Arrays of Nanofibers of Poly(vinylidenefluoride-co-trifluoroethylene). *Nat. Commun.* **2013**, *4*, 1633.

(22) Schwartz, G.; Tee, B. C.-K.; Mei, J.; Appleton, A. L.; Kim, D. H.; Wang, H.; Bao, Z. Flexible Polymer Transistors with High Pressure Sensitivity for Application in Electronic Skin and Health Monitoring. *Nat. Commun.* **2013**, *4*, 1859.

(23) Shin, S.-H.; Ji, S.; Choi, S.; Pyo, K.-H.; An, B. W.; Park, J.; Kim, J.; Kim, J.-Y.; Lee, K.-S.; Kwon, S.-Y.; Heo, J.; Park, B.-G.; Park, J.-U. Integrated Arrays of Air-Dielectric Graphene Transistors as Transparent Active-Matrix Pressure Sensors for Wide Pressure Ranges. *Nat. Commun.* **2017**, *8*, 14950.

(24) Wong, R. D. P.; Posner, J. D.; Santos, V. J. Flexible Microfluidic Normal Force Sensor Skin for Tactile Feedback. *Sens. Actuators, A* **2012**, *179*, 62−69.

(25) Dobrzynska, J. A.; Gijs, M. A. M. Flexible Polyimide-Based Force Sensor. *Sens. Actuators, A* **2012**, *173*, 127.

(26) Muhammad, H. B.; Recchiuto, C.; Oddo, C. M.; Beccai, L.; Anthony, C. J.; Adams, M. J.; Carrozza, M. C.; Ward, M. C. L. A Capacitive Tactile Sensor Array for Surface Texture Discrimination. *Microelectron. Eng.* **2011**, *88*, 1811−1813.

(27) Chortos, A.; Bao, Z. Skin-Inspired Electronic Devices. *Mater. Today* **2014**, *17*, 321.

(28) Zhao, X.; Hua, Q.; Yu, R.; Zhang, Y.; Pan, C. Flexible, Stretchable and Wearable Multifunctional Sensor Array as Artificial Electronic Skin for Static and Dynamic Strain Mapping. *Adv. Electron. Mater.* **2015**, *1*, 1500142.

(29) Yang, W.; Li, N.-W.; Zhao, S.; Yuan, Z.; Wang, J.; Du, X.; Wang, B.; Cao, R.; Li, X.; Xu, W.; Wang, Z. L.; Li, C. A Breathable and Screen-Printed Pressure Sensor Based on Nanofiber Membranes for Electronic Skins. *Adv. Mater. Technol.* **2017**, *3*, 1700241.

(30) Park, S.; Kim, H.; Vosgueritchian, M.; Cheon, S.; Kim, H.; Koo, J. H.; Kim, T. R.; Lee, S.; Schwartz, G.; Chang, H.; Bao, Z. Stretchable Energy-Harvesting Tactile Electronic Skin Capable of Differentiating Multiple Mechanical Stimuli Modes. *Adv. Mater.* **2014**, *26*, 7324−7332.

(31) Wang, X.; Gu, Y.; Xiong, Z.; Cui, Z.; Zhang, T. Silk-Molded Flexible, Ultrasensitive, and Highly Stable Electronic Skin for Monitoring Human Physiological Signals. *Adv. Mater.* **2014**, *26*, 1336−1342.

(32) Jian, M.; Xia, K.; Wang, Q.; Yin, Z.; Wang, H.; Wang, C.; Xie, H.; Zhang, M.; Zhang, Y. Flexible and Highly Sensitive Pressure Sensors Based on Bionic Hierarchical Structures. *Adv. Funct. Mater.* **2017**, *27*, 1606066.

(33) Craig, J. C.; Baihua, X. Temporal Order and Tactile Patterns. *Percept. Psychophys.* **1990**, *47*, 22−34.

DOI: 10.1021/acsami.9b02518
ACS Appl. Mater. Interfaces 2019, 11, 21218−21226

(34) Chung, J. Y.; Youngblood, J. P.; Stafford, C. M. Anisotropic Wetting on Tunable Micro-Wrinkled Surfaces. *Soft Matter* **2007**, *3*, 1163−1169.
(35) Someya, T.; Kato, Y.; Sekitani, T.; Iba, S.; Noguchi, Y.; Murase, Y.; Kawaguchi, H.; Sakurai, T. Conformable, Flexible, Large-Area Networks of Pressure and Thermal Sensors with Organic Transistor Active Matrixes. *Proc. Natl. Acad. Sci. U.S.A.* **2005**, *102*, 12321−12325.
(36) Lipomi, D. J.; Vosgueritchian, M.; Tee, B. C.-K.; Hellstrom, S. L.; Lee, J. A.; Fox, C. H.; Bao, Z. Skin-like pressure and strain sensors based on transparent elastic films of carbon nanotubes. *Nat. Nanotechnol.* **2011**, *6*, 788−792.
(37) Titze, I. R. The Human Instrument. *Sci. Am.* **2008**, *298*, 94−101.
(38) Titze, I. R. *Principles of Voice Production*; Prentice Hall, 1994.
(39) Cretikos, M. A.; Bellomo, R.; Hillman, K.; Chen, J.; Finfer, S.; Flabouris, A. Respiratory Rate: the Neglected Vital Sign Medical. *Med. J. Aust.* **2008**, *188*, 657.
(40) Barret, K. E.; Barman, S. M.; Boitano, S.; Brooks, H. *Ganong's Review of Medical Physiology*, 23rd ed.; McGraw-Hill Medical: NY, 2009.

DOI: 10.1021/acsami.9b02518
ACS Appl. Mater. Interfaces 2019, 11, 21218−21226